PHYTOCHROME INTERACTING FACTOR 7 moderates the activity and the cytosolic-nuclear shuttling of PHYTOCHROME A

Mengke Zhou[1*], Andrés Romanowski[2], Karen J. Halliday[1*]

1. Institute for Molecular Plant Sciences, School of Biological Sciences, University of Edinburgh, Edinburgh EH9 3BF, United Kingdom.

2. Timing of Environmental Signalling lab, Molecular Biology Group, Plant Sciences, Wageningen University & Research, Wageningen, The Netherlands.

ORCID IDs: 0000-0003-1043-2766 (MK. Z); 0000-0003-0737-2408(A.R.); 0000-0003-0467-104X (K.J.H.).

*Corresponding authors:
Mengke Zhou and Karen J. Halliday
Institute for Molecular Plant Sciences, School of Biological Sciences, University of Edinburgh, Edinburgh EH9 3BF, United Kingdom
+44-0131-651-9083
mengke.zhou@ed.ac.uk
karen.halliday@ed.ac.uk

ABSTRACT

In nature, plants sense and navigate complex vegetative environments using the phytochrome (phy) photoreceptor-signalling system. The canopy adaptation strategy, elicited by phyA, and the shade avoidance syndrome, regulated by phyB, allow plants to adapt to diverse forms of vegetation shade. The phyA High Irradiance Response (HIR) mode, involving photocycle-coupled nuclear shuttling, is essential for detecting persistent far-red rich conditions typical of canopy or occlusive shade. Our research identifies PHYTOCHROME INTERACTION FACTOR 7 (PIF7) as a critical regulator of phyA function. We demonstrate PIF7ox can effectively block phyA action. In persistent shade, PIF7 and phyA both accumulate and interact within nuclear bodies, with binding facilitated through the prion-like domain of PIF7 and the C-terminal PAS-PAS domain of phyA. PIF7 also interacts with FHY1 and FHL chaperones, interfering with phyA cytosolic-nuclear shuttling. This strategic molecular targeting by PIF7 provides an effective strategy for modulating the phyA HIR in response to shade signals.

INTRODUCTION

Light sensing is fundamental for plant adaptation and survival in vegetative shade. This is particularly important during seedling establishment, a stage when plants are most vulnerable. Plants have evolved distinct developmental strategies to cope with different types of shade that are prevalent in nature. The light receptor phytochrome B (phyB), is able to detect FR-rich light from neighbouring plants and elicit the Shade Avoidance Syndrome (SAS), which induces elongation of seedling hypocotyls, repositions leaves to improve light capture, and triggers early flowering [1,2]. Under persistent canopy shade, plants adopt alternative strategies, such as the phyA-mediated Canopy Adaptation Strategy (CAS), which suppresses hypocotyl elongation and conserves resources, optimising growth when shade is unyielding[3]. As vegetative habitats can change considerably through a season, the ability to adjust photoreceptor activity offers adaptive flexibility, ensuring successful seedling establishment and progression through the life cycle.

In Arabidopsis, phytochromes A-E, form a family of photoreceptors that principally absorb light in the red (R) and far-red (FR) regions of the spectrum[4]. Absorption of R, photoconverts phytochrome into its active Pfr form, while FR photoconverts Pfr to the inactive Pr conformer.

When activated phytochromes move from the cytosol to the nucleus where they aggregate in sub-nuclear photobodies to perform a range of functions[5,6]. While all phytochromes possess similar photosensory properties, they fall into two classes based on their distinct modes of action. Phytochromes B-E, which operate in the low fluence response (LFR) mode, are activated by R and deactivated by FR light. Consequently, in FR-rich vegetation shade environments, these phytochromes are less active[4,7]. A key distinction of phyA is that it is activated by FR-rich light through its high irradiance response (HIR) mode of action[7]. This property arises partly from its photobiology and partly from the shuttling mechanism that concentrates phyA in the nucleus[8]. PhyA lacks a nuclear localisation signal and primarily relies on the chaperone proteins FHY1/FHL to facilitate its transport into the nucleus. These proteins specifically recognise phyA-Pfr and transport it to the nucleus, where it is converted into phyA-Pr, allowing FHY1/FHL to dissociate and be recycled to the cytoplasm for further shuttling[8,9,10]. Nuclear located phyA regulates a number of processes, including expression of target genes, through association with transcription factors such as PHYTOCHROME INTERACTING FACTORS (PIFS) and ELONGATED HYPOCOTYL 5 (HY5)[11]. The central role of FHY1/FHL shuttling in the phyA HIR, identifies this mechanism as a potential target for modifying phyA action and the adaptive response[8]. Indeed, HY5 has been reported to be involved in negative-feedback regulation of phyA signalling through repressing FHY1/FHL expression[11]. Here HY5 directly interacts with the DNA-binding regions of FAR-RED ELONGATED HYPOCOTYLS 3 (FHY3) and FAR-RED IMPAIRED RESPONSE 1 (FAR1) to prevent their transcriptional activation of FHY1/FHL.

PIF transcription factors are well-studied negative regulators of phytochrome signalling that. They function by directly binding to G/PBE-boxes in the promoters of their target genes[12]. In Arabidopsis, there are eight PIFs (PIF1, PIF2/PIL1-PIF8), each with an active phytochrome B (APB) domain that facilitates their interaction with phyB. Only PIF1 and PIF3 contain an active phytochrome A (APA) domain, which directly binds the C-terminus of phyA, comprising two Period-Arnt-SIM (PAS) and a histidine kinase-related (HKRD) domains[13]. In FR light phyA directly interacts with PIF1 and PIF3 triggering their proteolytic destruction and/or sequestration from target promoters[13,14]. Although PIF4, PIF5, PIF8 and PIF7 lack an APA

domain, they have been shown to controls aspects of phyA signalling[15,16,17]. Interestingly, levels of PIF8 protein are boosted by phyA. In darkness COP1 (CONSTITUTIVE PHOTOMORPHOGENESIS 1) promotes PIF8 protein degradation through the 26S proteasome, thereby reducing its abundance. Conversely, under FR light, phyA inhibition of COP1 stabilises the PIF8 protein, forming a negative feedback loop that limits phyA action[15].

Notably, PIF7, a close homologue of PIF8, is a potent regulator of SAS. In unshaded conditions, PIF7 interacts with active phyB (Pfr) through its APB domain, and both proteins localise to sub-nuclear photobodies. This interaction prevents PIF7 from binding to the promoters of target genes, effectively inhibiting PIF7-regulated gene expression[18,19]. Under shade conditions, the deactivation of phyB releases PIF7 from this repression, leading to the activation of shade-responsive genes and triggering the physiological SAS response[20,21]. Furthermore, exposure to shade triggers the dephosphorylation and nuclear accumulation of PIF7, processes that enhance the activation of SAS[20]. Given its strong promotory role in SAS, it is notable that PIF7 has recently been demonstrated to increase *PHYA* transcript abundance, an action that could potentially limit SAS. This PIF7 action can be inhibited by *PHYA UTR ANTISENSE RNA (PUAR),* which binds to PIF7 and prevents its interaction with the 5' UTR, thereby reducing *PHYA* transcript levels[17]. Collectively, this research underscores the importance of PIF7 as a key agent in executing and moderating the molecular response to shade.

Our study substantially deepens our understanding of PIF7's role in modulating phyA signalling. We have demonstrated that overexpression of PIF7 (PIF7ox) can completely negate the suppressive effects of phyA on seedling hypocotyl elongation in persistent shade. Under these conditions, PIF7 and phyA co-localize in nuclear photobodies, where they directly interact. This interaction is facilitated by the prion-like domain of PIF7 and the C-terminus of phyA. Additionally, our results reveal that PIF7 crucially governs the subcellular localisation of phyA, a process mediated by the chaperone proteins FHY1 and FHL. These findings elucidate the molecular mechanism whereby PIF7 concurrently limits phyA nuclear transport and signalling.

RESULTS

105 **PIF7ox blocks phyA action**

106 PIF7, which functions downstream of phyB, also shares significant sequence similarity with
107 PIF8, a regulator of phyA responses. This similarity led us to investigate the potential genetic
108 interaction between PIF7 and phyA. To do this we assessed hypocotyl length in seedlings grown
109 in 8h white light (WL): 16h dark (D) or in 8h low R:FR ratio (0.2) light (WLFR) photoperiods,
110 which commenced one day after germination to elicit a strong phyA response (Fig. 1a). As
111 expected, wild type (WT, *Col-0*) seedlings were slightly shorter in WLFR compared to WL,
112 while *phyA-211* had longer hypocotyls in WLFR due to reduced control of shade-avoidance
113 elongation (Fig. 1b-c). In contrast, the phyAox line displayed a constitutively short hypocotyl
114 and retained WLFR-responsivity. In WL the *pif7-1, pif7-2* loss-of-function alleles were
115 marginally shorter than the WT but retained a response to WLFR that was absent in the *pif7-1*;
116 *phyA-211* double mutant. In keeping with PIF7's function in promoting the phyB-mediated
117 shade response, under WLFR, *pif7-1* diminishes the impact of *phyA-211* on hypocotyl length.
118 Conversely, hypocotyls of 35S:PIF7-FLASH (PIF7ox) seedlings were elongated in WL and
119 exhibited further elongation under WLFR. As hypocotyl lengths were similar in PIF7ox and
120 PIF7ox;*phyA-211,* this suggests PIF7ox facilitates increased shade-avoidance elongation while
121 simultaneously suppressing phyA action (Fig. 1c)[18]. This observation infers PIF7 may
122 participate in phyB to phyA cross-regulation.

123 Given the capacity of PIF7ox to inhibit phyA activity, we sought to investigate the possibility
124 of functional redundancy with other PIFs. As anticipated, PIF8ox also lacked WLFR-mediated
125 growth inhibition, but PIF3ox, PIF4ox and PIF5ox all retained this response (Fig. S1a-b)[15]. Our
126 data therefore illustrate that even though PIF3, PIF4 and PIF5 have been implicated in *PHYA*
127 regulation and signalling, their functions diverge from PIF7 and PIF8[16,22,23]. We found the
128 hypocotyl lengths of *pif8-1* and *pif8-1;phyA-211* were qualitatively similar to *pif7-1, pif7-2*, and
129 *pif7-1;phyA-211*, respectively (Fig. S1c). However, comparison of the *PIF7ox;phyA-211* and
130 *PIF8ox;phyA-211* lines reveal distinct differences in PIF7 and PIF8. While PIF7ox is epistatic
131 to *phyA-211*, this genetic relationship shifts for PIF8, particularly under WLFR, where we show
132 *phyA-211* is epistatic to PIF8ox. This finding aligns well with evidence showing PIF8 functions

133 downstream of phyA[15].

134 In summary, our findings show PIF7 has a distinct role in antagonising the suppression of
135 hypocotyl growth by phyA, a phenomenon particularly evident in the PIF7ox lines, which
136 effectively block this response.

137 **PIF7 moderates phyA protein abundance**

138 PIF7 is known to promote shade induction of *PHYA* expression by binding to 5' UTR[17].
139 Concurring with this study, we found that when sampled one hour before dusk (ZT7) in an
140 8L:16D photoperiod, WLFR enhanced *PHYA* expression in the WT, whereas this response was
141 diminished in the *pif7-1* mutant. Likewise, PIF7ox exhibited elevated *PHYA* levels in control
142 conditions which were further enhanced in WLFR (Fig. 1d). Immunoblot analysis using an
143 antibody against native phyA, reported phyA levels to be consistently low in WL, across all
144 genotypes. We observed that WLFR led to an increase in phyA protein levels in WT, *pif7-1* and
145 PIF7ox, which qualitatively corresponded with the patterns seen in *PHYA* mRNA data (Fig. 1e-
146 f). Further, we found that PIF7ox had a negligible effect on the phyApr:phyA-nLUC (phyA-
147 nLUC) in WL, which is known to gradually deplete under these conditions. In-line previous
148 studies, we observed higher levels of daytime phyA-nLUC in WLFR, which was notably
149 elevated by PIF7ox (Fig. 1g)[3]. Collectively, these findings demonstrate that under WLFR
150 conditions, PIF7 regulates *PHYA* expression and the abundance of phyA protein. Interestingly,
151 despite PIF7ox accumulating significantly higher levels of phyA under WLFR, PIF7ox
152 seedlings fail to elicit a phyA response. This indicates that the regulatory effect of PIF7 on phyA
153 activity does not stem from changes in phyA abundance.

154 To examine the *in vivo* dynamics of PIF7 under our experimental conditions we generated
155 PIF7pr:PIF7-nLUC (PIF7-nLUC) lines. We discovered that PIF7-nLUC exhibits rhythmic
156 patterns, with higher levels during the day compared to the night (Fig. S2 a). WLFR boosted
157 daytime levels of PIF7-nLUC levels, with the *phyA-211* mutation elevating PIF7-nLUC toward
158 the end of the period, especially in WLFR (Fig. S2 b). Therefore, our data indicate that similar
159 to phyA, WLFR increases the abundance of PIF7, and that phyA plays a minor role in reducing

160 PIF7 production toward the end of the photoperiod.

161 **PIF7 can interact with phyA in nuclear photobodies**

162 To establish whether PIF7 and phyA interact *in planta* we first used 35S:PIF7-sfGFP (PIF7-
163 GFP) and 35S:phyA-RFP (phyA-RFP) transiently expressed in *N. bethamina* leaves to establish
164 whether PIF7 are found in the same cellular location. We found that following WLFR treatment
165 PIF7-GFP and phyA-RFP co-localise in nuclei and in sub-nuclear foci, or photobodies (Fig. 2a).
166 Quantitative fluorescence measurements along a nuclear transect, intersecting two photobodies,
167 clearly shows this co-localisation (Fig. 2a). Next, we created split bimolecular fluorescence
168 complementation (BiFC) constructs 35S:PIF7-nYFP and 35S:phyA-cYFP, to test whether PIF7
169 and phyA physically interact *in vivo*. In WLFR, BiFC assays yielded strong nuclear, and sub-
170 nuclear foci signals, but not in control lines expressing 35S:PIF7-nYFP and 35S:EV-cYFP. The
171 data suggest PIF7 and phyA are indeed able to interact in nuclei and within photobodies under
172 WLFR (Fig. 2b).

173 To gain further evidence for this interaction we also generated split nanoLUC (nLUC) luciferase
174 reporter constructs, 35S:PIF7-lgbitnLUC (PIF7-lgbit) and 35S:phyA-smbitnLUC (phyA-
175 smbit), with 35S:phyB-smbitnLUC (phyB-smbit) and 35S:phyA-nLUC (phyA-nLUC) as
176 controls (Fig. 2c). As expected, we found a strong signal in the PIF7-lgbit+phyB-smbit in WL
177 which is diminished in WLFR, which is consistent with the known light conditional interaction
178 between PIF7 and phyB[18]. Again, as expected we observed a strong signal from phyA-nLUC
179 in WLFR, which is known to increase phyA abundance, while negative controls (phyA-smbit+
180 phyB-smbit) had low signal in both conditions. In WL conditions, the signal from PIF7-lgbit +
181 phyA-smbit was low, similar to that of the negative control, whereas in WLFR conditions, the
182 signal was strong, indicating an interaction. Further, using an antibody to native phyA we
183 demonstrated co-immunoprecipitation of phyA with PIF7ox, in WLFR but not WL conditions
184 (Fig. 2d). Thus, our data provides evidence that PIF7 and phyA directly interact in photobodies
185 after exposure to WLFR which promotes their respective nuclear accumulation[20,24].

186 **Prion-like Domain of PIF7 interacts with phyA PAS-PAS Domain**

187 Earlier work demonstrated that phyA binds directly with PIF1 and PIF3. The phyA C-terminal
188 output module (OPM) is known to be important for this interaction, as is the active phyA-
189 binding domains (APA) of PIF1 and PIF3[13,22]. To identify PHYA regions that required for the
190 molecular interaction we utilised PIF7-nYFP and phyA-cYFP split YFP assay, creating
191 truncated PHYA constructs as follows: C-terminal (phyA-C), comprising HINGE (H), PAS-
192 PAS DOMAIN (PAS), and HISTIDINE KINASE RELATED DOMAIN (HKRD) regions
193 [H+PAS+HKRD-cYFP], phyA-C1 [PAS+HKRD-cYFP], phyA-P [PAS-cYFP], and phyA-H
194 [HKRD-cYFP] (Fig. 3a). In WLFR we obtained nuclear fluorescence signals for PIF7-nYFP
195 and the full-length phyA-cYFP control, as well as the truncated phyA-C, phyA-C1, and phyA-
196 P constructs. No signal was observed for phyA-H and the negative EV control. The strong signal
197 detected for phyA-P, which includes PAS-PAS domain motifs, highlights the significance of
198 this molecular region in facilitating the interaction with PIF7. To identify the region of PIF7
199 that mediated the interaction with phyA, we generated PIF7-N which contains the ACTIVE
200 PHYTOCHROME BINDING domain [PIF7-N-nYFP], PIF7-B, containing the BASIC
201 HELIX-LOOP-HELIX motif [PIF7-N-nYFP], and PIF7-C which contains a Prion-like domain
202 (PrLD) [PIF7-C-nYFP] which has a polyQ-rich sequence is located at PrLD center (Fig. 3b,
203 Fig. S6). Interestingly we found that only the PIF7 full length control and PIF7-C gave nuclear
204 fluorescence in WLFR. Thus, our data point to the prion-like domain of PIF7 as being important
205 for its interaction with phyA. Since PIF7 lacks an APA domain, it seems that prion region is
206 able to fulfill this role.

207 **PIF7 regulates the subcellular localisation of phyA**

208 Our data show PIF7ox elevates phyA protein levels, yet PIF7ox lines are unable to mount a
209 phyA response in WLFR conditions. As WLFR drives the phyA HIR and its nuclear
210 accumulation, we sought to analyse cellular location more closely. As anticipated, confocal
211 microscopy revealed strong cytosolic and weaker nuclear signals for phyA-GFP
212 (phyApr:phyA-sGFP), and for GFP-PIF7 (35S:GFP-PIF7) when in WL (Fig. S3). Exposure to
213 WLFR notably enhanced nuclear relative to cytosolic signals, confirming the nuclear
214 accumulation of both PIF7 and phyA under our shade conditions (Fig. S3a)[19,20,25]. We then

215 aimed to establish if PIF7 affected the location of phyA by introgressing phyA-GFP into *pif7-*
216 *1* and PIF7ox backgrounds. In WL we found phyA-GFP to be predominantly in the cytosol in
217 Col-0, *pif7-1* and PIF7ox lines (Fig. 4a). Under WLFR, we recorded a higher proportion of
218 nuclear phyA-GFP in WT, especially in *pif7-1*, while significantly lower levels were observed
219 in PIF7ox (Fig. 4b-c). Thus, PIF7 appears to influence the cytoplasmic to nuclear partitioning
220 of phyA-GFP. To verify our results, we performed immunoblot assays that differentiated
221 between nuclear and cytosolic fractions. This method yielded qualitatively similar results
222 showing increased nuclear phyA in *pif7-1* and predominately cytosolic PHYA in PIF7ox (Fig.
223 4d-e). Thus, our findings indicate that PIF7 modifies subcellular phyA localization. The notably
224 reduced nuclear presence of phyA in PIF7ox could partially account for the disrupted phyA
225 signaling observed in PIF7ox.

226 **PIF7ox blocks phyA regulation of target genes**

227 To further interrogate the mechanism through which PIF7 inhibits phyA action we initially
228 tested whether PIF7 alters the expression of genes (*CHS, BIN2, FHY3, FHY1*, *FHL* and *IAA29)*
229 known to be directly regulated by phyA (Fig. 5a)[26,27]. As determined by qPCR all the genes,
230 except *IAA29*, were upregulated in WT in WLFR conditions, otherwise, the expression patterns
231 fell into two categories. In WLFR conditions, *CHS, BIN2,* and *FHY3* exhibited decreased
232 expression in both *phyA-211* and PIF7ox, while their expression was increased in *pif7-1*. This
233 gene set is upregulated by phyA in WLFR, and their expression is repressed by PIF7. On the
234 other hand, *FHY1, FHYL* and *IAA29* form a group that are upregulated in *phyA-211* and PIF7ox,
235 and for *FHY1* and *FHYL*, expression is lowered in *pif7-1*. These genes are downregulated by
236 phyA in WLFR, and their expression is promoted by PIF7. The common factor for all these
237 genes is that phyA and PIF7 exert opposing control of their regulation, particularly in WLFR.

238 We then sought to establish if the antagonistic action of PIF7 was mediated through direct
239 repression of phyA at target gene promoters. Here we performed chromatin
240 immunoprecipitation (ChIP) using a native phyA antibody, and qPCR using to detect phyA
241 enrichment at *CHS, FHY1*, and *FHL* promoters (Fig. 5b). For all three genes we found WLFR
242 stimulated phyA enrichment at promoter regions sequences containing G-box motifs (two in

243 CHS), but not in G-box-free regions (Control, coding region). This enrichment was eliminated
244 in the presence of PIF7ox, suggesting the interaction between PIF7 and phyA is able to block
245 phyA regulation of target genes.

246 **PIF7 interacts with FHY1 and FHL**

247 In WLFR phyA cytosolic to nuclear shuttling is controlled by FHY1 and FHL chaperones[9]. The
248 central importance of this mechanism for phyA function is evident in the *fhy1-3;fhl-1* double
249 mutant hypocotyl response which is phenotypically similar to *phyA-211* (Fig. S4). An intriguing
250 finding of our study is that PIF7 appears to control the subcellular location of phyA. We
251 therefore wanted to establish if this arose through a process involving PIF7 interaction with
252 FHY1 and FHL. Using the *N. benthamiana* transient expression system, we recorded nuclear
253 interactions between the BiFC constructs 35S:FHY1-cYFP, 35S:FHL-cYFP, and 35S:PIF7-
254 nYFP under WLFR conditions (Fig. 6a). We also observed PIF7 interactions with FHY1 and
255 FHL, but not the negative control using a split nLUC assay (Fig. 6b). It is worth noting that in
256 this assay the interaction signal strength between the shuttle proteins and PIF7 was lower than
257 that for PIF7 and phyA (Fg. 6b). However, we were able to verify these interactions through
258 co-immunoprecipitation using 35S:FHY1/FHL-nLUC and 35S:PIF7-sfGFP (Fig 6c). As our
259 data shows PIF7 is able to interact with phyA, FHY1 and FHL, we postulated that these proteins
260 may form a complex under inductive WLFR conditions. Supporting this hypothesis, we found
261 that when FHY1-YFP or FHL-YFP are co-expressed with PIF7-sfGFP and phyA-RFP in *N.*
262 *benthamiana* leaves, these constructs localise to the same nuclear regions under WLFR (Fig.
263 6d-e).

264 Another factor worth considering is *ARABIDOPSIS SUMO PROTEASE 1 (ASP1)*, which plays
265 an important role in SUMOylation and maintaining FHY1 levels under FR light conditions[28].
266 We observed increased levels of *ASP1* expression in PIF7ox compared to WT in WL. We found
267 *ASP1* levels are enhanced by WLFR, a response that is further amplified by *pif7-1* and
268 suppressed by PIF7ox (Fig. 6f). Thus, PIF7 regulation of *ASP1* may contribute to its regulation
269 of the shuttling mechanism.

To determine if PIF7 primarily acts by sequestering phyA or whether the PIF7 interactions with FHY1/FHL are also important, we employed phyApr:phyA-sGFP-NLS (phyA-NLS), where phyA is constitutively nuclear (Fig S7)[29]. In line with earlier findings, under our experimental conditions, phyA-NLS restores the *phyA-201* elongated hypocotyl phenotype to WT length (Fig. 6g). We hypothesised that if PIF7 regulation of phyA was solely due to its sequestration of phyA, then PIF7ox should diminish the function of phyA-NLS through this mechanism[29]. However, our data show phyA-NLS exhibits strong epistasis over PIF7ox, for hypocotyl length, and the expression of *CHS* and *IAA29* under WLFR (Fig. 6g, S5). Consequently, it seems that the mechanism of phyA sequestration alone likely cannot explain the potent effects of PIF7ox on phyA action. Previous research demonstrated that phyA-NLS completely restores phyA control of hypocotyl growth in *fhy1-3;fhl-1 and phyA-211;fhy1-3;fhl-1*, indicating that phyA-NLS can bypass the requirement for nuclear shuttling[30]. Consequently, our results imply that the interaction between PIF7 and FHY1/FHL may be required to suppress phyA action. Under WLFR, the transport of phyA into the nucleus is highly dynamic. Therefore, PIF7 may interact with phyA-FHY1/FHL complexes soon after their nuclear entry and before the complexes disassemble. This scenario is consistent with our co-localisation data (Fig.6d)[9]. Collectively, our data indicates that PIF7 forms inactive complexes with phyA and FHY1/FHL, which simultaneously impedes phyA shuttling and signalling.

DISCUSSION

The operating properties of phyA are distinct from other phytochromes. Under shaded conditions, phyA requires a cytosolic to nuclear shuttling mechanism to operate effectively, a process facilitated by the chaperone proteins FHY1 and FHL. In this study, we have shown PIF7 is a potent regulator of this process, limiting the availability of phyA for signalling. The impact on phyA is most extreme in the PIF7ox line, where WLFR-induced phyA action is blocked. Our research illustrates that PIF7 moderates phyA intracellular movement and signalling through molecular sequestration.

Studies have shown that both PIF7 and phyA accumulate in the nucleus under FR-rich shade conditions[31,18,29]. Our findings further reveal that PIF7-GFP and phyA-RFP co-localise to

298 specific sub-nuclear foci, where they physically interact as evidenced by BiFC (Fig.2a-b).
299 Additional confirmation of this interaction was provided by split nLUC assays employing PIF7-
300 lgbit and phyAsmbit, along with co-immunoprecipitation of PIF7ox and phyA.

301 While all PIFs have an active phytochrome B (APB) domain that enables binding to phyB, only
302 PIF1 and PIF3 have active phytochrome A (APA) motifs, through which they interact with the
303 phyA C-terminus[15,32]. This binding is known to facilitate the proteolysis of PIF1 and PIF3, and
304 to inhibit the activity of PIF3 by isolating it from target promoters[15,32,33]. Our research has
305 demonstrated that although PIF7 lacks an APA domain, it can still directly interact with phyA.
306 This binding is facilitated through the PAS domain of phyA and the C-terminal region of PIF7,
307 which contains a prion-like domain. PIF7 moderates the activity of phyA by inhibiting its ability
308 to bind to target promoters (Fig. 5b). For the genes *CHS*, *FHY3*, and *BIN2*, which are activated
309 by phyA in WLFR, and for *FHY1*, *FHL*, *IAA29*, which are repressed by phyA, PIF7 counteracts
310 the effects of phyA.

311 PIF7 is particularly effective in FR-rich shade, which triggers its dephosphorylation, increases
312 its abundance, and enhances its accumulation in nuclear photobodies (Fig. S3b)[20]. Shade also
313 deactivates phyB, which typically limits the DNA-binding capacity of PIF7[19]. Since continuous
314 shade also stimulates phyA activity, it creates conducive conditions for the interaction between
315 PIF7 and phyA.

316 We have demonstrated that PIF7 and phyA interact within sub-nuclear structures known as
317 photobodies[5]. These photobodies are essentially molecular condensates that form through
318 liquid-liquid phase separation (LLPS), accompanied by a nucleation step. Nucleation aids
319 sequestration, particularly at low concentrations, and targets the formation of photobodies to
320 specific sub-nuclear sites[6,34]. Across organisms, the spatial organisation of biomolecules into
321 distinct cellular locations is essential for enabling specialised functions[35].

322 PIF7 is unique amongst PIF proteins as it contains a prion-like domain with a central polyQ
323 stretch of 17 consecutive glutamine residues. PIF8 is the closest in sequence similarity to PIF7,
324 and while does possess a short polyQ sequence in its C-terminus, this domain exhibits low
325 prion-like predictability (Fig.S6). Prion-like domains (PrLD) typically comprise low-

complexity or intrinsically disordered regions that facilitate protein condensation and LLPS. Indeed, PIF7 is able to form condensates with LLPS characteristics *in vitro*, which is proposed to facilitate the formation of PIF7-phyB photobodies[19]. Substituting polyQ with polyA diminishes the capacity of PIF7 to form photobodies, highlighting the importance of polyQ in this process. Interestingly, phyB has also been shown to possess LLPS characteristics, for its C-terminus, and disordered N-terminal extension have both been shown to phase-separate in mammalian cells[36]. We have shown that in WLFR, PIF7 interacts with the phyA, through its PrLD, which results in the formation of PIF7-phyA-containing photobodies. Within these biomolecular condensates, phyA-mediated signalling and control of hypocotyl growth are suppressed. In the PIF7ox line, this inhibition results in excessive elongation of the hypocotyl under WLFR, since PIF7 action is no longer constrained by phyA.

The movement of phyA to the nucleus in WLFR is strongly contingent on the chaperone proteins FHY1 and FHL7. Through the use of BiFc, split nanoLUC and co-immunoprecipitation assays, we demonstrated that PIF7 also interacts with FHY1 and FHL under WLFR. Fluorescent tagged versions of PIF7, phyA and FHY1/FHL illustrated that these proteins co-localise within nuclei, suggesting the formation of PIF7-phyA-FHY1/FHL complexes. Nuclear shuttling of phyA is a highly dynamic process that operates continuously under WLFR conditions[9,37]. Earlier work indicates that dissociation of the phyA-FHY1/FHL complex is required to both recycle the shuttle proteins and to facilitate phyA signalling[31,37]. We therefore propose that PIF7 may serve to trap phyA and FHY1/FHL in inactive complexes, which simultaneously perturbs the nuclear transport of phyA and disconnects it from downstream signalling. Consistent with this interpretation, we find *pif7-1* and PIF7ox have higher proportions of nuclear, and cytosolic phyA, respectively (Fig. 4b-e). Further, our genetic data shows that phyA-NLS, which is constitutively nuclear, and bypasses the FHY1/FHL shuttling mechanism, can restore phyA function to PIF7ox in WLFR, in terms of hypocotyl phenotype and *CHS* and *IAA29* gene expression (Fig. 6g, Fig. S5). We also discovered that PIF7 reduces the expression of *ARABIDOPSIS SUMO PROTEASE 1 (ASP1)*, which aids the deSUMOylation of FHY1 under FR light, thereby preventing its degradation. *ASP1* suppression may, therefore, represent an alternative mechanism through which PIF7 modulates phyA

shuttling. Previously, our research demonstrated that under simulated shade, PIF7 interacts with and suppresses the transcriptional activity of ANGUSTIFOLIA 3 (AN3), a promoter of leaf cell proliferation[38]. In this case, PIF7 operates by evicting and substituting for AN3 at target promoters. Thus, in shade conditions, PIF7 assembles different nuclear complexes which execute distinct functions.

In summary, our study outlines the central role PIF7 plays in regulating phyA activity. Its direct binding to phyA, and the FHY1/FHL chaperones, likely represents a rapid, energy-efficient, and highly effective way to stem phyA action. The compartmentalisation of phyA and FHY1/FHL into PIF7 photobodies constitutes a dynamic regulatory mechanism that responds to changes in environmental light quality. This subcellular partitioning enables PIF7 to drive hypocotyl elongation while simultaneously reducing the suppressive influence of phyA. Since the modulation of PIF7 by phyB is well-established, our findings position PIF7 at the molecular intersection of phyB and phyA, underscoring its pivotal role in adjusting phyA activity to promote SAS elongation under vegetative shade[19].

METHODS

Plant material and growth conditions

The wild-type of *Arabidopsis thaliana* seedlings are Columbia-0 (*Col-0*). The *pif7-1*, *pif7-2*[39], *pif8-1*, *pif8-2* mutants, and the construction of *pif8-1;phyA-211*, *PIF8ox;phyA-211* and PIF8OX[15], PIF7OX-FLASH[40], 35S:GFP-PIF7[20], 35S:PIF3-LUC[41], 35S:PIF5-HA, 35S:PIF4-LUC[16], phyApr:phyA-sGFP, phyApr:phyA-sGFP-NLS[25], and phyApr:phyA-nanoLUCx3FLAGx10His (phyA-nLUC)[3] have been described previously. The *phyA-211* mutant was obtained from NASC collection. PIF7pr:PIF7-nanoLUCx3FLAGx10His (PIF7-nLUC) (Basta) were transformed into the *pif7-1* background. The *pif7-1*;phyA-sGFP-NLS, and PIF7ox;phyA-sGFP-NLS, *pif7-1*;*phyA-211* and PIF7ox;*phyA-211* lines were generated by genetic crossing. Likewise, the *pif7-1;*phyA-nLUC, PIF7ox;phyA-nLUC, PIF7pr:PIF7-nLUC; *phyA-211* lines were made through genetic crossing. All the cross lines were verified using PCR or sequencing.

382 For the hypocotyl growth experiments seeds were first sterilized and then re-suspended in 0.1%
383 (w/v) agar and stored in darkness at 4°C for 3 d to stratify. Following this, seeds were
384 individually sown onto plates containing half-strength Murashige and Skoog basal salts mixture
385 (Duchefa Biochemie, Haarlem, Netherlands) dissolved in 1% (w/v) agar (1/2 MS media; pH
386 5.8). The plates were then transferred to Percival I30BLL growth chambers at 22 °C (Plant
387 Climatics, Wertingen, Germany). To promote germination seeds were exposed to a 4 h period
388 of white light (WL) (85±5 μmol m^{-2} s^{-1}), and then darkness for 20 h, before transferring to
389 experimental photoperiods. For all experiments seedlings were grown under short day (8L:16D)
390 conditions in either WL or WL with supplementary FR (WLFR) to provide a R:FR ratio of 0.20.

391 **RNA extraction and q-PCR**

392 For RNA extraction seedlings (n = 36 ± 5 seedling numbers), were harvested at Zeitgeber time
393 7 (ZT) which is one hour before dark. Total RNA was extracted using a phenol-based method[38],
394 300 μL RNA extraction buffer (PH=8.0) was added to each sample, followed by 300 μL 1:1
395 acidic phenol: chloroform. The supernatant was separated from the pellet by centrifuging for
396 15 minutes at 13,000 rpm under 4°C. Up to 300 μL of the supernatant was transferred to
397 collection tubes with 240 μL isopropanol and 30 μL 3 M sodium acetate. Samples were
398 precipitated at -80°C for 15 minutes, then centrifuged for 30 minutes at 13,000 rpm. Pellets
399 were washed with 300 μL of 70% ethanol and then suspended in nuclease free water and stored
400 at -80°C. Complementary DNA (cDNA) synthesis was performed using the qScript cDNA
401 SuperMix (Quanta Biosciences) as described by the manufacturer. A Lightcycler 480 system
402 (Roche) was employed for real time-qPCR, with 10 μL reactions that incorporated the SYBR
403 Green Master Mix (Roche). The q-PCR primers are shown in **Supplementary table 2**. Results
404 were analysed using Light Cycler 480 (Roche).

405 **Hypocotyl measurements and statistical analysis**

406 Images of hypocotyls were taken after a period of 6 days growth, and hypocotyl length was
407 analysed using ImageJ (https://imagej.nih.gov/ij/). Data analysed by Excel and GraphPad Prism
408 10. Data are presented as mean values ± s.e.m. Two-way ANOVA (α=0.05) was conducted to
409 assess statistical significance across light conditions for each genotype; asterisks denote
410 significance relative to control treatments: 0.1234 (ns), 0.0332 (*), 0.0021 (**), 0.0002 (***),
411 P < 0.0001 (****). Representative data from three independent replicates are shown.

412 **Construct assembly**

413 The full-length CDS of *phyA* and nanoLUC tag (NLUCx3FLAGx10His; NL3F10H) have been
414 described previously[3]. The CDS of *PIF7* were synthesised by the GeneArt Gene Synthesis

service (Invitrogen, MA, USA). The split nanoLUC tags were made by splitting nanoLUC to lgbit (158 aa) and smbit (11 aa). Mobius Assembly[42] was used to insert the constructs into a mUAV plasmid (L0, CamR) with *AraI* restriction site and plasmid assembly was performed and subsequently verified by the Edinburgh Genome Foundry. The full-length CDS of *FHY1* and *FHL* parts were amplified with Q5 High-Fidelity DNA polymerase (New England Biolabs, MA, USA) from the *Col-0* genome by gene-specific primers. The phyA-C, phyA-C1, phyA-P, phyA-H, PIF7-N, PIF7-B and PIF7-C part cloned on the CDS region of *phyA* and *PIF7* (L0 parts). These parts were assembled into a mUAV plasmid and sequenced by Source Bioscience (Cambridge, UK). All L0 parts will assemble in pMAP B L1 (KamR) vector with *BsaI* restriction site. All the constructs for the tobacco (*Nicotiana benthamiana*) assay used a CaMV35S promoter, which is synthesized by the GeneArt Gene Synthesis service (Invitrogen, MA, USA).

To construct pEXP601- PIF7pr:PIF7-nanoLUCx3FLAGx10His, a 2740 bp genomic fragment was generated, encompassing the PIF7 promoter region (1015 bp), 5'UTR (161 bp), and 1564 bp ORF, excluding the stop codon of exon 6 of the AT5G61270.1. This fragment was PCR-amplified using specific primers with Phusion High-Fidelity DNA Polymerase (NEB, M0530S). The resulting amplicon was subsequently recombined into pDONR221 using BP II clonase (Invitrogen, 12535029), and its sequence verified by Sanger sequencing (Genepool, Edinburgh Genomics, Edinburgh, UK). The genomic regions were then recombined into pGWB601: NanoLUC-3FLAG-10His sing LR Clonase (Invitrogen)[43]. The final construct was transformed into Agrobacterium AGL1. Primer used for construct assembly are listed in **Supplementary table 1.**

The Tobacco Transient Expression Assay

The CaMV35S constructs were transferred into the Agrobacterium AGL1 strain and cultured at 28°C for two days, before infiltration into 4-week-old *Nicotiana benthamiana* leaves. Agrobacterium expression construsts was infiltrated into *Nicotiana benthamiana* leaves with P19. The solution used for transient expression experiments contained 10 mM MES buffer (pH 5.6), 10 mM $MgCl_2$ and 200 mM aceto-syringone. Plants were grown under short day (8L:16D, at 22°C) conditions in either WL or WL with supplementary FR (WLFR) to provide a R:FR ratio of 0.20. Tobacco will used for next step after 3 days treatments.

Confocal Imaging, Colocalization, and BiFC

The fluorescence images of GFP, YFP and RPP expression were obtained with a Leica confocal micro-scope (Leica SP8) at 488 and 552 nm laser. For BiFC and co-localization assay all images

were taken at ZT7 on day 3 after WL/WLFR treatments. The co-localization signals were analysed by LAS X Office 1.4.7.2982 and plotted by GraphPad Prism 10. phyApr:phyA-sGFP(NLS), *pif7-1*;phyA-GFP, PIF7ox;phyA-GFP and 35S:GFP-PIF7 transgenic lines images were taken at ZT7 within 30 minutes after 6 days of WL/WLFR treatments. The Nuclear and cytosolic signals were quantified from cells in the mid-hypocotyl region within a 20 x 1.36 objective lens. Nucleus and cytoplasmic signals were quantified using Image J and plotted in GraphPad Prism 10. Imaging experiment comprised three biological replicates, with 6 seedlings in each replicate.

Immunoblot Analysis and Co-immunoprecipitation Assays

Each sample comprised 0.5-1 g of Arabidopsis seedling tissue, harvested on day 6 at ZT7. Samples were added to lysis buffer (125 mM Tris-HCl (pH 7.5); 0.25mM EDTA (pH 7.5), 150 mM NaCl, 5% glycerol, 0.1% Triton X-100, 0.5% NP-40), which contained 1X Protease inhibitor (Sigma-Aldrich, P9599) and 1x HALT-Phosphatase inhibitor (Thermo Scientific). Samples were centrifuged at 12,000 rpm for 10 mins at 4ºC and then transferred to lysate mix with 1x SDS loading buffer (containing 0.1 M DTT) at a 1:1 volume ratio. Samples were incubated at 80ºC for 10 mins, followed by a centrifugation step, prior to western blotting.

For Co-immunoprecipitation, after lysis an aliquot of the total protein was saved as an input sample. Then other total protein extracts were incubated with Protein A/G beads (MCE Magnetic Agarose) for 1 h at 4 C to remove adventitious binding proteins. Then anti-FLAG/His beads (Anti-FLAG M2 agarose gel Sigma-Aldrich, Cat.No. A2220; Anti-His Magnetic Beads, Cat. 209, MCE) added into treated protein extracts over night at 4ºC. The antibody/protein complex was washed with wash buffer (125 mM Tris-HCl [pH 7.5]; 0.25mM EDTA [pH 7.5], 150 mM NaCl, 5% glycerol, 0.1 % Triton X-100) 5 times. Then added 50 µL of 1x SDS loading buffer to each sample and incubate at 80ºC for 8 mins.

To detect phyA protein, an anti-Phytochrome A antibody (PHYTOAB, PHY1907) was used at 1:1,000. To detect the PIF7OX-FLASH and 35S:FHY1/FHL-nanoLUC x3FLAGx10His an anti-FLAG M2 antibody (Sigma-Aldrich, F1804) was used at 1:2,000. To detect the 35S:PIF7-sfGFP an anti-GFP anti-body (Roche, ab290) was used at 1:3,000. Anti-RPN6 antibody (Agrisera, AS121858) was used at 1:3,000 as internal control. Secondary antibodies (1:3,000, anti-mouse IgG (cell signalling, 7076s); 1:4,000 Goat anti-rabbit-IgG (Abcam, AB6013) were used for the ECL Prime Western Blotting System. The signals were detected by Azure 300 Imager with ECL prime western blotting detection reagents (Cytiva, RPN2232).

NanoLUC and split nanoLUC assays

481 NanoLUC bioluminescence assays were conducted as previously described[3]. Add in each well
482 of. Single Arabidopsis seedlings were grown in individual wells, in a 96 well plate, each
483 containing 200 µl 1/2 MS media. Plates were sealed with cling film and placed under 8L:16D
484 (WL) for 6 days. Before imaging 50 µl diluted (1:50) of Nano-Glo (Promega, Nano-
485 Glo®Luciferase Assay) was added to the seedlings in each well. Plates were sealed and moved
486 to experimental light conditions. Bioluminescence was recorded every hour (for 1.5 s) for
487 several days using the TriStar2 LB942 multimode microplate reader (Berthold Technologies,
488 Germany). The data was analysed and plotted using BioDare2 software[44] and Excel. Typically,
489 9 biological repeats were conducted with at least 6 seedlings per replicate in **Fig.1g**.

490 The split nanoLUC assay is like BIFC assay method. Through Agrobacterial infiltrated into
491 *Nicotiana benthamiana* leaves. After 3 days WL/WLFR treatments, the 1cm x 1cm size leaves
492 will be used in 96 wells plates (*n* =12 leaf numbers) for collecting signals. Next add 100 µl
493 diluted (1:50) Nano-Glo on the top of the leaves to each well. Then the signals will collect by
494 plate reader. The data analysed by Excel and GraphPad Prism 10. The experiments repeated at
495 least 3 times and had similar results.

496 **Chromatin Immunoprecipitation (ChIP)-qPCR**

497 We employed ChIP-qPCR methods described by previews work, as follows[45]. For each sample
498 0.5-1g of tissue was extracted from 6 day -old seedlings at ZT7. Cross-linking was induced
499 with 1% formaldehyde under vacuum infiltration for 15 mins (up to -70 kPa), then 2.5 ml of 2
500 M glycine was added to quench crosslinking. DNA was fragmented into an average size of
501 ~150 bp in Diagenode BioRuptor Plus, (30 cycles of high power 30s ON / 30s OFF). Anti-
502 phyA antibody (PHYTOAB, PHY1907,1:300) incubated with protein A/G beads (MCE
503 Magnetic Agarose) in 4°C overnight. And the following day samples were incubated with
504 protein A/G bead/phyA antiboday complex for 6 hours at 4°C. DNA was extracted using
505 phenol/chloroform (1:1, vol/vol). Protein enrichment at DNA regions was quantified using RT-
506 qPCR using primers detailed in **Supplementary table 2.** Enrichment was determined
507 by %Input method (%Input=2 ^ [CtInput-CtChIP] × IDF × 100%).

508 **Nuclear-Cytoplasmic Fractionation**

509 Nuclear fractionation was performed essentially as previously described with the following
510 modifications[46]. Briefly, 0.5-1 g of Arabidopsis seedlings ground into fine powder in liquid
511 nitrogen and then homogenised in double the volume of pre-cooled (4°C) lysis buffer (20 mM
512 Tris-HCl, pH 7.4, 25% Glycerol, 20 mM KCl, 2 mM EDTA, 2.5 mM MgCl2, 250 mM Sucrose
513 and 5 mM DTT, add 1×protease inhibitor cocktail (Roche) and 1 x HALT-Phosphatase inhibitor
514 added in fresh). The sample was filtered twice through two layers of Mira cloth (Merck

Millipore). The flow-through was spun 10 min at 2000g, 4°C. Supernatant, consisting of the cytoplasmic fraction, was centrifuged 20 min at 13,000g, 4°C and collected. The pellet, containing the nuclear fraction, was washed six times with 2.5 mL of nuclear resuspension buffer NRBT1 (20 mM Tris-HCl, pH 7.4, 25% Glycerol, 2.5 mM $MgCl_2$, 0.2% Triton X-100) and centrifuged 3 min at 1,500g, 4°C. The pellet was resuspended in 300 µL of pre-cooled NRBT2 (250 mM Sucrose, 10 mM Tris-HCl, pH 7.5, 10 mM MgCl2, 1% Triton X-100, 0.035% β-mercaptoethanol ,and 1× protease inhibitor cocktail added in fresh), and carefully overlaid on top of 300 µL NRBT3(1.7 M Sucrose, 10 mM Tris-HCl, pH 7.5, 2 mM MgCl2, 0.15% Triton X-100, 0.035% β-mercaptoethanol, and 1× protease inhibitor cocktail added in fresh). These were centrifuged at 16,000g for 55 min at 4°C, and the final nuclear pellet was resuspended in 2× SDS loading buffer. As quality controls for the fractionation, RbCL (Agrisera, AS03037, 1:3,000) protein was used as the cytoplasmic control, and histone H3 (Abcam, ab18521, 1:3,000)) was used as the nuclear control in immunoblot assays.

ACKNOWLEDGEMENTS

This research was supported by University of Edinburgh Darwin Trust Scholarship awarded to MK. Z and Leverhulme Trust grant RPG-2024-082 awarded to K.J.H. We thank Dr. Rist Van de Weyer who generated PIF7ox;*phyA-211* and first observed the PIF7ox hypocotyl phenotype in WLFR. We thank Prof. Lin Li, Prof. Dr. Andreas Hiltbrunner and Dr. Gabriela Toledo-Ortiz who kindly shared 35S:GFP-PIF7, 35S:phyA-RFP and phyApr:phyA-sGFP(NLS) seeds and thank Prof. Giltsu Choi for sharing *pif8-1;phyA-211*, *PIF8ox;phyA-211* and PIF8OX lines.

AUTHOR CONTRIBUTIONS

MK. Z and K.J.H. planned and designed the research. MK. Z performed and analysed all experiments with K.J.H. A.R. generated the PIF7pr:PIF7-nanoLUC line. MK. Z and K.J.H. both contributed to manuscript preparation.

REFERENCE

1 Liu, Y., Jafari, F. & Wang, H. Y. Integration of light and hormone signaling pathways in the regulation of plant shade avoidance syndrome. *Abiotech* **2**, 131-145 (2021). https://doi.org:10.1007/s42994-021-00038-1.

2 Franklin, K. A. Shade avoidance. *New Phytol* **179**, 930-944 (2008). https://doi.org:10.1111/j.1469-8137.2008.02507.x.

3 Butlin, P., Valdivia-Cabrera, M., Grima, R. & Halliday, K. J. Arabidopsis thaliana Phytochrome A Sensory Properties in Canopy Shade. *bioRxiv* (2025). https://doi.org:10.1101/2025.05.14.654025.

4 Mathews, S. & Sharrock, R. A. Phytochrome gene diversity. *Plant Cell Environ* **20**, 666-

549 671 (1997). https://doi.org:10.1046/j.1365-3040.1997.d01-117.x.
550 5 Cheng, M. C., Kathare, P. K., Paik, I. & Huq, E. Phytochrome Signaling Networks. *Annu*
551 *Rev Plant Biol* **72**, 217-244 (2021). https://doi.org:10.1146/annurev-arplant-080620-
552 024221.
553 6 Du, J., Kim, K. & Chen, M. Distinguishing individual photobodies using Oligopaints
554 reveals thermo-sensitive and -insensitive phytochrome B condensation at distinct
555 subnuclear locations. *Nature Communications* **15** (2024). https://doi.org:10.1038/s41467-
556 024-47789-1.
557 7 Casal, J. J., Luccioni, L. G., Oliverio, K. A. & Boccalandro, H. E. Light, phytochrome
558 signalling and photomorphogenesis in. *Photoch Photobio Sci* **2**, 625-636
559 (2003).https://doi.org:10.1039/b300094j.
560 8 Rausenberger, J. *et al.* Photoconversion and Nuclear Trafficking Cycles Determine
561 Phytochrome A's Response Profile to Far-Red Light. *Cell* **146**, 813-825 (2011).
562 https://doi.org:10.1016/j.cell.2011.07.023.
563 9 Hiltbrunner, A. *et al.* Nuclear accumulation of the phytochrome A photoreceptor requires
564 FHY1. *Curr Biol* **15**, 2125-2130 (2005). https://doi.org:10.1016/j.cub.2005.10.042.
565 10 Genoud, T. *et al.* FHY1 Mediates Nuclear Import of the Light-Activated Phytochrome A
566 Photoreceptor. *Plos Genet* **4** (2008). https://doi.org:10.1371/journal.pgen.1000143.
567 11 Li, J. G. *et al.* Transcription Factor ELONGATED HYPOCOTYL5 Plays a Role in the
568 Feedback Regulation of Phytochrome A Signaling. *Plant Cell* **22**, 3634-3649 (2010).
569 https://doi.org:10.1105/tpc.110.075788.
570 12 Pham, V. N., Kathare, P. K. & Huq, E. Phytochromes and Phytochrome Interacting Factors.
571 *Plant Physiol* **176**, 1025-1038 (2018). https://doi.org:10.1104/pp.17.01384.
572 13 Jeong, J., Lee, Y. & Choi, G. Both phytochrome A and phyB interact with
573 PHYTOCHROME-INTERACTING FACTORs through an evolutionary conserved
574 phy(OPM)-APA interaction. *Nat Commun* **16**, 3946 (2025).
575 https://doi.org:10.1038/s41467-025-59327-8.
576 14 Al-Sady, B., Ni, W., Kircher, S., Schafer, E. & Quail, P. H. Photoactivated phytochrome
577 induces rapid PIF3 phosphorylation prior to proteasome-mediated degradation. *Mol Cell*
578 **23**, 439-446 (2006). https://doi.org:10.1016/j.molcel.2006.06.011.
579 15 Oh, J., Park, E., Song, K., Bae, G. & Choi, G. PHYTOCHROME INTERACTING
580 FACTOR8 Inhibits Phytochrome A-Mediated Far-Red Light Responses in Arabidopsis.
581 *Plant Cell* **32**, 186-205 (2020). https://doi.org:10.1105/tpc.19.00515.
582 16 Seaton, D. D. *et al.* Dawn and photoperiod sensing by phytochrome A. *P Natl Acad Sci*
583 *USA* **115**, 10523-10528 (2018). https://doi.org:10.1073/pnas.1803398115.
584 17 Zhu, T., Yang, C., Xie, Y., Huang, S. & Li, L. Shade-induced lncRNA PUAR promotes
585 shade response by repressing PHYA expression. *EMBO Rep* **24**, e56105 (2023).
586 https://doi.org:10.15252/embr.202256105.
587 18 Leivar, P. *et al.* The Arabidopsis phytochrome-interacting factor PIF7, together with PIF3
588 and PIF4, regulates responses to prolonged red light by modulating phyB levels. *Plant*
589 *Cell* **20**, 337-352 (2008). https://doi.org:10.1105/tpc.107.052142.
590 19 Xie, Y. *et al.* Phytochrome B inhibits the activity of phytochrome-interacting factor 7
591 involving phase separation. *Cell Rep* **42** (2023).
592 https://doi.org:10.1016/j.celrep.2023.113562.

20 Huang, X. *et al.* Shade-induced nuclear localization of PIF7 is regulated by phosphorylation and 14-3-3 proteins in Arabidopsis. *Elife* **7** (2018). https://doi.org:10.7554/eLife.31636.

21 Park, E. *et al.* Phytochrome B inhibits binding of phytochrome-interacting factors to their target promoters. *Plant Journal* **72**, 537-546 (2012). https://doi.org:10.1111/j.1365-313X.2012.05114.x.

22 Ni, M., Tepperman, J. M. & Quail, P. H. PIF3, a phytochrome-interacting factor necessary for normal photoinduced signal transduction, is a novel basic helix-loop-helix protein. Cell 95, 657-667 (1998). https://doi.org:10.1016/S0092-8674(00)81636-0.

23 Lorrain, S., Trevisan, M., Pradervand, S. & Fankhauser, C. Phytochrome interacting factors 4 and 5 redundantly limit seedling de-etiolation in continuous far-red light. *Plant Journal* **60**, 449-461 (2009). https://doi.org:10.1111/j.1365-313X.2009.03971.x.

24 Kevei, E., Schafer, E. & Nagy, F. Light-regulated nucleo-cytoplasmic partitioning of phytochromes. *J Exp Bot* **58**, 3113-3124 (2007). https://doi.org:10.1093/jxb/erm145.

25 Toledo-Ortiz, G. *et al.* Subcellular sites of the signal transduction and degradation of phytochrome A. *Plant Cell Physiol* **51**, 1648-1660 (2010). https://doi.org:10.1093/pcp/pcq121.

26 Chen, F. *et al.* Phosphorylation of FAR-RED ELONGATED HYPOCOTYL1 is a key mechanism defining signaling dynamics of phytochrome A under red and far-red light in Arabidopsis. *Plant Cell* **24**, 1907-1920 (2012). https://doi.org:10.1105/tpc.112.097733.

27 Wang, H. & Deng, X. W. Arabidopsis FHY3 defines a key phytochrome A signaling component directly interacting with its homologous partner FAR1. *EMBO J* **21**, 1339-1349 (2002). https://doi.org:10.1093/emboj/21.6.1339.

28 Qu, G. P. *et al.* Reversible SUMOylation of FHY1 Regulates Phytochrome A Signaling in Arabidopsis. *Mol Plant* **13**, 879-893 (2020). https://doi.org:10.1016/j.molp.2020.04.002.

29 Toledo-Ortiz, G. *et al.* Subcellular sites of the signal transduction and degradation of phytochrome A. *Plant Cell Physiol* **51**, 1648-1660 (2010). https://doi.org:10.1093/pcp/pcq121.

30 Menon, C., Klose, C. & Hiltbrunner, A. Arabidopsis FHY1 and FHY1-LIKE Are Not Required for Phytochrome A Signal Transduction in the Nucleus. *Plant Commun* **1**, 100007 (2020). https://doi.org:10.1016/j.xplc.2019.100007.

31 Rausenberger, J. *et al.* Photoconversion and Nuclear Trafficking Cycles Determine Phytochrome A's Response Profile to Far-Red Light. *Cell* **146**, 813-825 (2011). https://doi.org:10.1016/j.cell.2011.07.023.

32 Al-Sady, B., Ni, W., Kircher, S., Schafer, E. & Quail, P. H. Photoactivated phytochrome induces rapid PIF3 phosphorylation prior to proteasome-mediated degradation. *Mol Cell* **23**, 439-446 (2006). https://doi.org:10.1016/j.molcel.2006.06.011.

33 Shen, H. *et al.* Light-induced phosphorylation and degradation of the negative regulator PHYTOCHROME-INTERACTING FACTOR1 from depend upon its direct physical interactions with photoactivated phytochromes. *Plant Cell* **20**, 1586-1602 (2008). https://doi.org:10.1105/tpc.108.060020.

34 Kim, C. *et al.* Phytochrome B photobodies are comprised of phytochrome B and its primary and secondary interacting proteins. *Nature Communications* **14** (2023). https://doi.org:10.1038/s41467-023-37421-z.

35 Zhang, X. Y. *et al.* Liquid-liquid phase separation in diseases. *Medcomm* **5** (2024). https://doi.org:e64010.1002/mco2.640.

36 Chen, D. *et al.* Integration of light and temperature sensing by liquid-liquid phase separation of phytochrome B. *Mol Cell* **82**, 3015-+ (2022). https://doi.org:10.1016/j.molcel.2022.05.026.

37 Genoud, T. et al. FHY1 Mediates Nuclear Import of the Light-Activated Phytochrome A Photoreceptor. Plos Genet 4 (2008). https://doi.org:100014310.1371/journal.pgen.1000143.

38 Hussain, E., Romanowski, A. & Halliday, K. J. PIF7 controls leaf cell proliferation through an AN3 substitution repression mechanism. *P Natl Acad Sci USA* **119** (2022). https://doi.org:10.1073/pnas.2115682119.

39 Leivar, P. *et al.* Multiple Phytochrome-Interacting bHLH Transcription Factors Repress Premature Seedling Photomorphogenesis in Darkness. *Curr Biol* **18**, 1815-1823 (2008). https://doi.org:10.1016/j.cub.2008.10.058.

40 Li, L. *et al.* Linking photoreceptor excitation to changes in plant architecture. *Genes Dev* **26**, 785-790 (2012). https://doi.org:10.1101/gad.187849.112.

41 Viczián, A. *et al.* Functional characterization of phytochrome interacting factor 3 for the circadian clockwork. *Plant and Cell Physiology* **46**, 1591-1602 (2005). https://doi.org:10.1093/pcp/pci175.

42 Andreou, A. I. & Nakayama, N. Mobius Assembly: A versatile Golden-Gate framework towards universal DNA assembly. Plos One 13 (2018). https://doi.org:10.1371/journal.pone.0189892.

43 Urquiza-García, U. & Millar, A. J. Expanding the bioluminescent reporter toolkit for plant science with NanoLUC. Plant Methods 15 (2019). https://doi.org:10.1186/s13007-019-0454-4.

44 Zielinski, T., Moore, A. M., Troup, E., Halliday, K. J. & Millar, A. J. Strengths and Limitations of Period Estimation Methods for Circadian Data. *Plos One* **9** (2014). https://doi.org:10.1371/journal.pone.0096462

45 Wang, Z. S. *et al.* Proteasome-associated ubiquitin ligase relays target plant hormone-specific transcriptional activators. *Sci Adv* **8** (2022). https://doi.org:10.1126/sciadv.abn4466.

46 Zhu, D. M. *et al.* Biochemical Characterization of Complexes Containing CONSTITUTIVELY PHOTOMORPHOGENIC1 and SUPPRESSOR OF PHYA Proteins in Light Control of Plant Development. *Plant Cell* **20**, 2307-2323 (2008). https://doi.org:10.1105/tpc.107.056580.

47 Rosler, J., Klein, I. & Zeidler, M. double mutant reveals a distinct cytoplasmic action of phytochrome A. *P Natl Acad Sci USA* **104**, 10737-10742 (2007). https://doi.org:10.1073/pnas.0703855104.

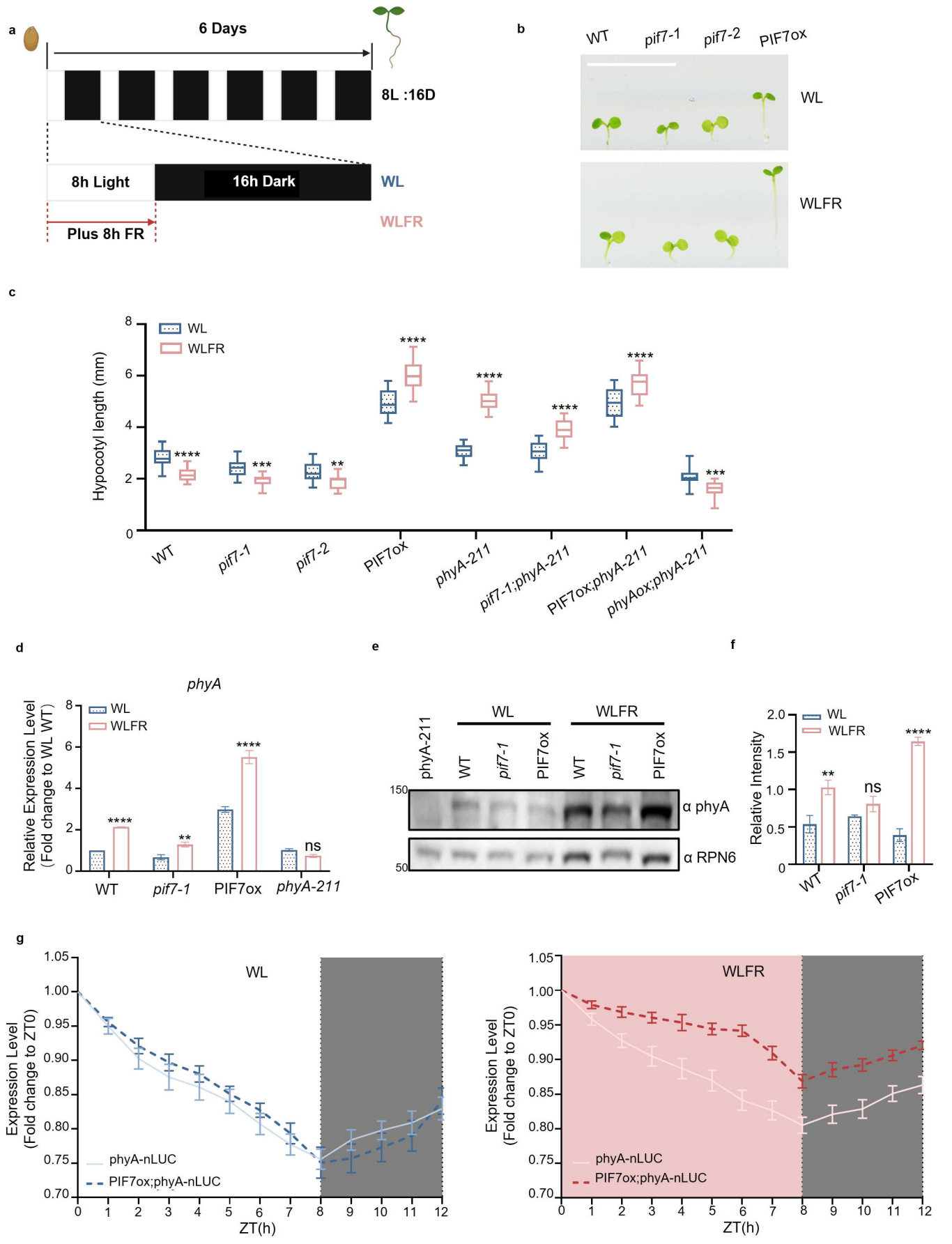

Fig. 1 PIF7ox influences phyA Function in WLFR

a, Schematic of experimental growth conditions. Seeds were sown on 1/2 MS plates and cultivated for one day under white light, followed by 4 hours (h) of light and 20 h of dark. Seedlings were subsequently grown for 6 days in white light (WL) photoperiods with or without supplementary far-red (WLFR), lowering the R:FR to 0.20 (red arrow). For all experiments, light regimes were 8 h light at PAR = 85 ± 5 μmol m^{-2} s^{-1}, 16 h dark, at 22°C.

b, Representative images of *Arabidopsis thaliana* WT (*Col-0*), *pif7-1*, *pif7-2*, and PIF7ox seedlings grown in WL or WLFR for 6 days. Scale bar = 1 cm.

c, PIF7ox blocks phyA action in WLFR. Hypocotyl length (mm) of WT (*Col-0*), *pif7-1*, *pif7-2*, PIF7ox, *phyA-211*, *pif7-1;phyA-211*, *PIF7ox;phyA-211* and phyAox under WL and WLFR. Representative images from three independent replicates are shown.

d, In WLFR, PIF7 enhances *PHYA* expression at Zeitgeber time 7 (ZT). Real-time qPCR was used to quantify *PHYA* mRNA levels, with *PP2A* as internal control. Samples were collected at ZT7 (1 hour before dusk) from 6d-old seedlings grown in WL or WLFR.

e,**f**, In WLFR, PIF7 increases phyA protein accumulation. PhyA protein levels were determined by immunoblotting. Anti-phyA was used to detect native phyA, while anti-RPN6 served as an internal control. The bar chart (**f**) displays the relative levels of phyA, normalised to RPN6, based on data from four biological replicates collected at ZT7.

g, PIF7ox boosts phyA protein levels in diel conditions. The phyA-nLUC line was generated by expressing (*PHYApr:phyA-nLUC*) in *phyA-211*, while the PIF7ox;phyA-nLUC was generated by introgressing *PHYApr:phyA-nLUC* into the PIF7ox line. Bioluminescence signals were recorded from day 6.

For **c**,**d**,**f**,**g**, data are presented as mean values ± s.e.m., *n*=25 (seedling numbers) in **c**; with *n*=3,4,9 (biological repeats) in **d**,**f**,**g**, respectively. For **c**,**d**,**f**, a Two-way ANOVA was conducted to assess statistical significance across light conditions for each genotype (α=0.05); asterisks denote significance relative to WL treatments: 0.1234 (ns), 0.0332 (*), 0.0021 (**), 0.0002 (***), $P <$ 0.0001 (****).

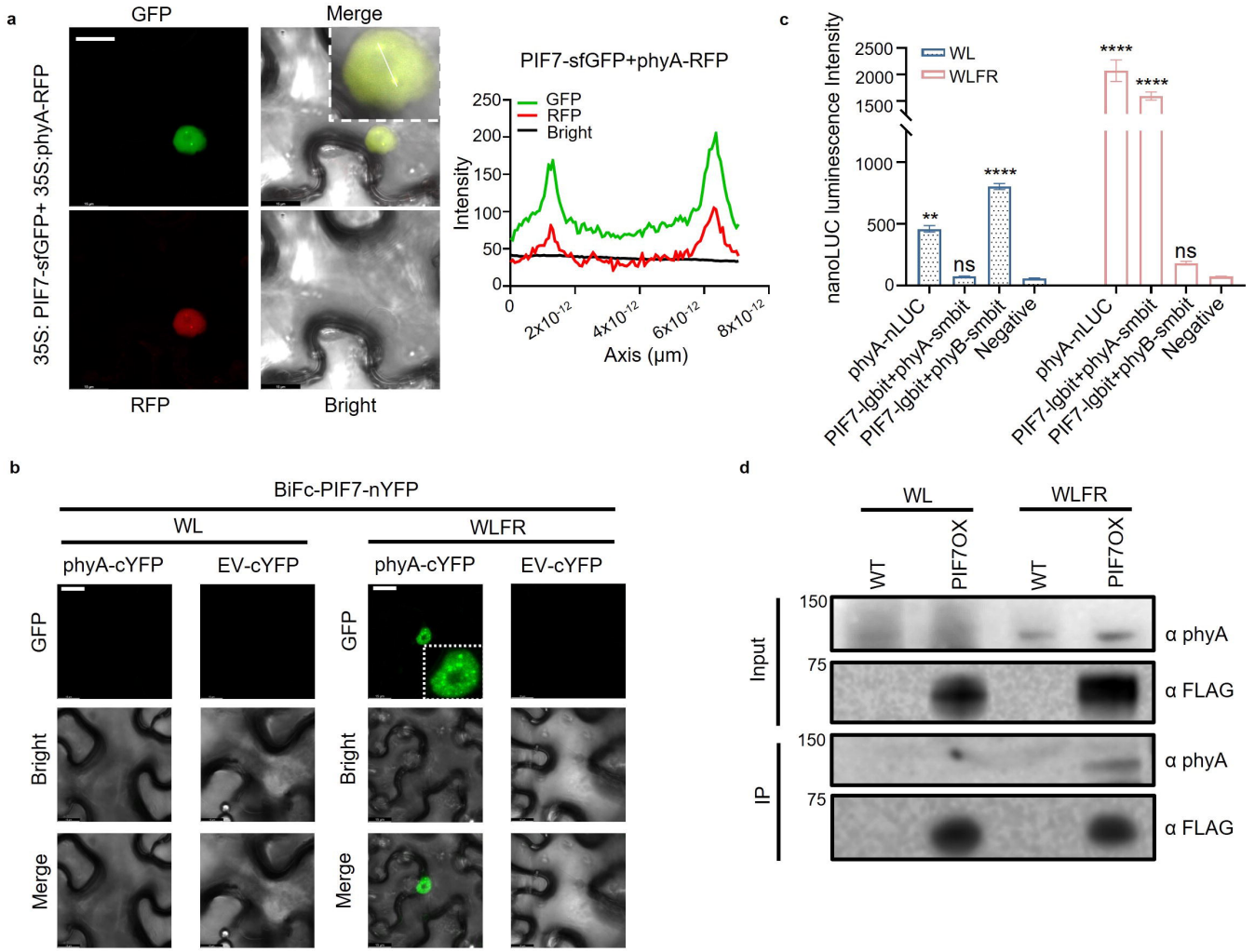

Fig. 2 PIF7 and phyA interact in sub-nuclear photobodies under WLFR.

a, 35S:PIF7-sfGFP and 35S:phyA-RFP co-localise in nuclei and photobodies in WLFR. Co-localisation is evident from the chart (right) which traces the GFP and RFP channel signals along the white bar shown in merged nucleus image (left).

b, Split NanoLUC (nLUC) assay demonstrates PIF7 and phyA physically interact. 35S:PIF7-lgbitnLUC (PIF7-lgbit), 35S:phyA-smbitnLUC (phyA-smbit), 35S:phyB-smbitnLUC (phyB-smbit) and 35S:phyA-nLUC (phyA-nLUC) reporter constructs were expressed in *Nicotiana benthamiana*. A WLFR-dependent interaction was demonstrated for PIF7-lgbit+phyA-smbit. PhyA-nLUC was used as light conditional controls, and phyB-smbit+phyA-smbit as the negative control.

c, Bimolecular Fluorescence Complementation (BiFC) assay confirms PIF7 and phyA interact in nuclear photobodies. BiFC was detected between 35S:PIF7-nYFP and 35S:phyA-cYFP (PIF7-nYFP + phyA-cYFP) in WLFR, but not with the 35S:EV-cYFP (EV-cYFP) control.

d, Co-immunoprecipitation assay (Co-IP) shows that phyA interacts with PIF7 in WLFR *in vivo*. Anti-His beads were used to pull down PIF7 from PIF7ox (35S:*PIF7-FLASH*; 9xMyc-6xHis-3xFlag) or the WT(*Col-0*) negative control. Anti-phyA and anti-FLAG used for detecting phyA and PIF7 respectively, in IP/Input. Samples were collected at ZT7 from 6-d old seedlings exposed to WL or WLFR.

For **a**,**c**, 488nm and 552nm laser detected the GFP/YFP and RFP signals. Scale Bar=15μm. For **b**, data are presented as mean values ± s.e.m., *n*=12 (leaf numbers). A Two-way ANOVA test was used to obtain statistical significance (α=0.05); asterisks denote statistical significance comparing negative to positive test or tested interaction treatments: 0.1234 (ns), 0.0332(*), 0.0021 (**), 0.0002(***), P<0.0001 (****). Representative images from three independent replicates are shown in all figs.

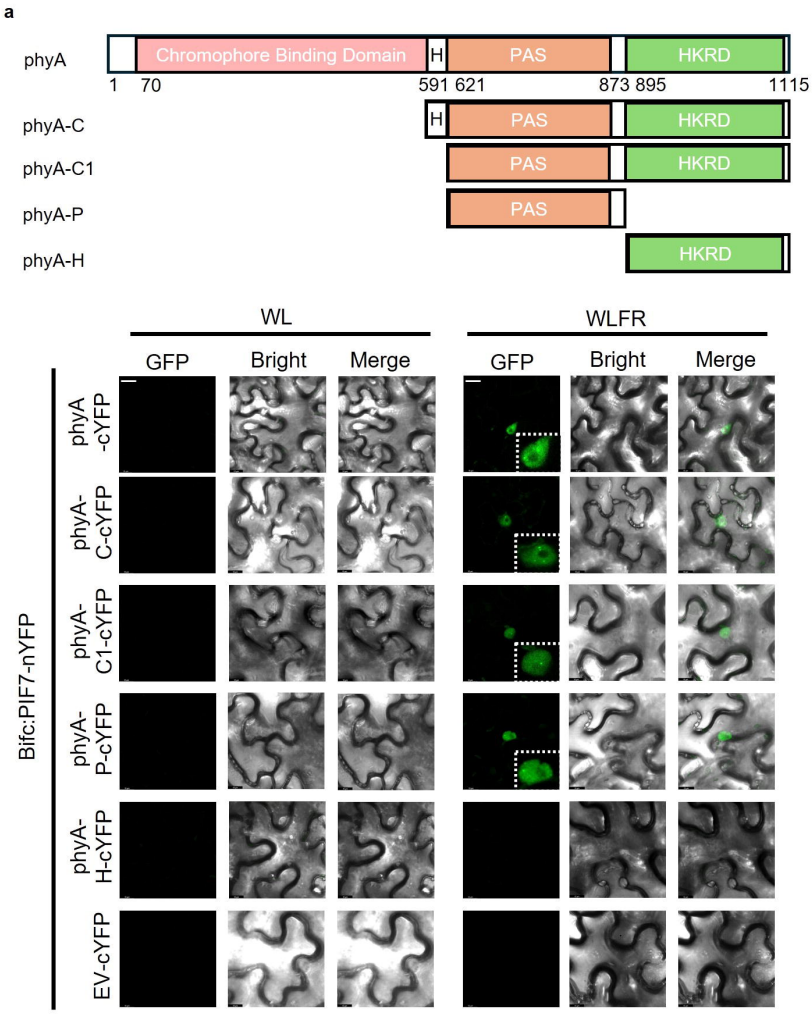

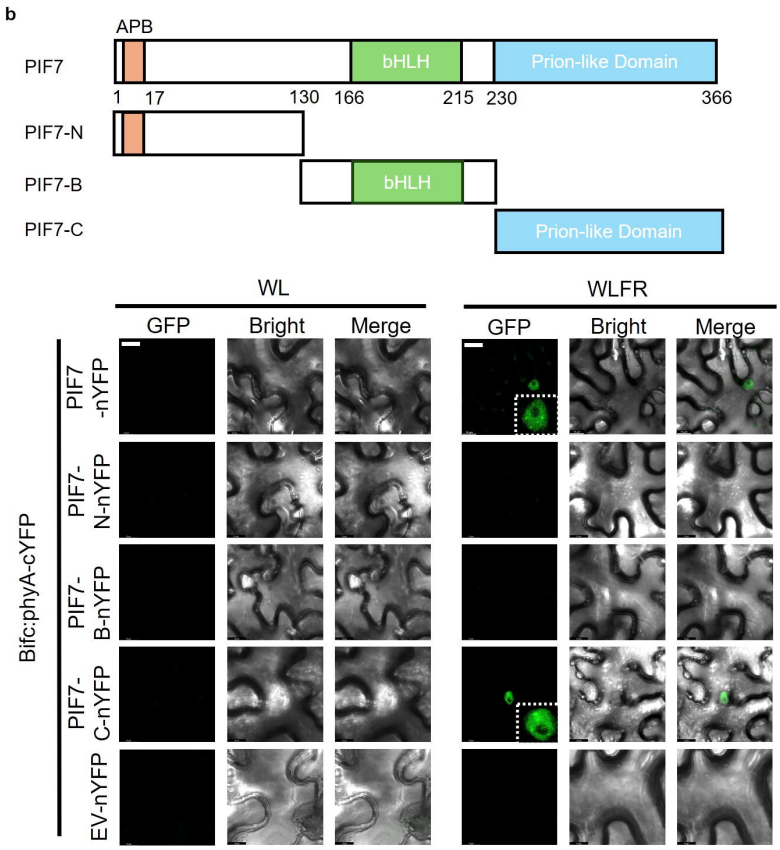

Fig. 3 The PIF7-phyA Interaction Depends on the PIF7 Prion like domain

a-b, BIFC assays using truncated constructs identify the phyA PAS domain and the PIF7 prion-like domain, as important for the phyA-PIF7 interaction. The constructs image depicted the complete phyA/PIF7 protein structures. Full length and truncated contructs were fused to C-terminal nYFP (PIF7) or cYFP (phyA) BIFC constructs. PIF7-nYFP+phyA-cYFP was used as positive control and 35S:EV-cYFP/35S:EV-nYFP (EV-cYFP/EV-nYFP) as used as negative controls. 488nm lasers were used to detect the YFP signals. Scale Bar=15μm. Representative images from three independent replicates are shown.

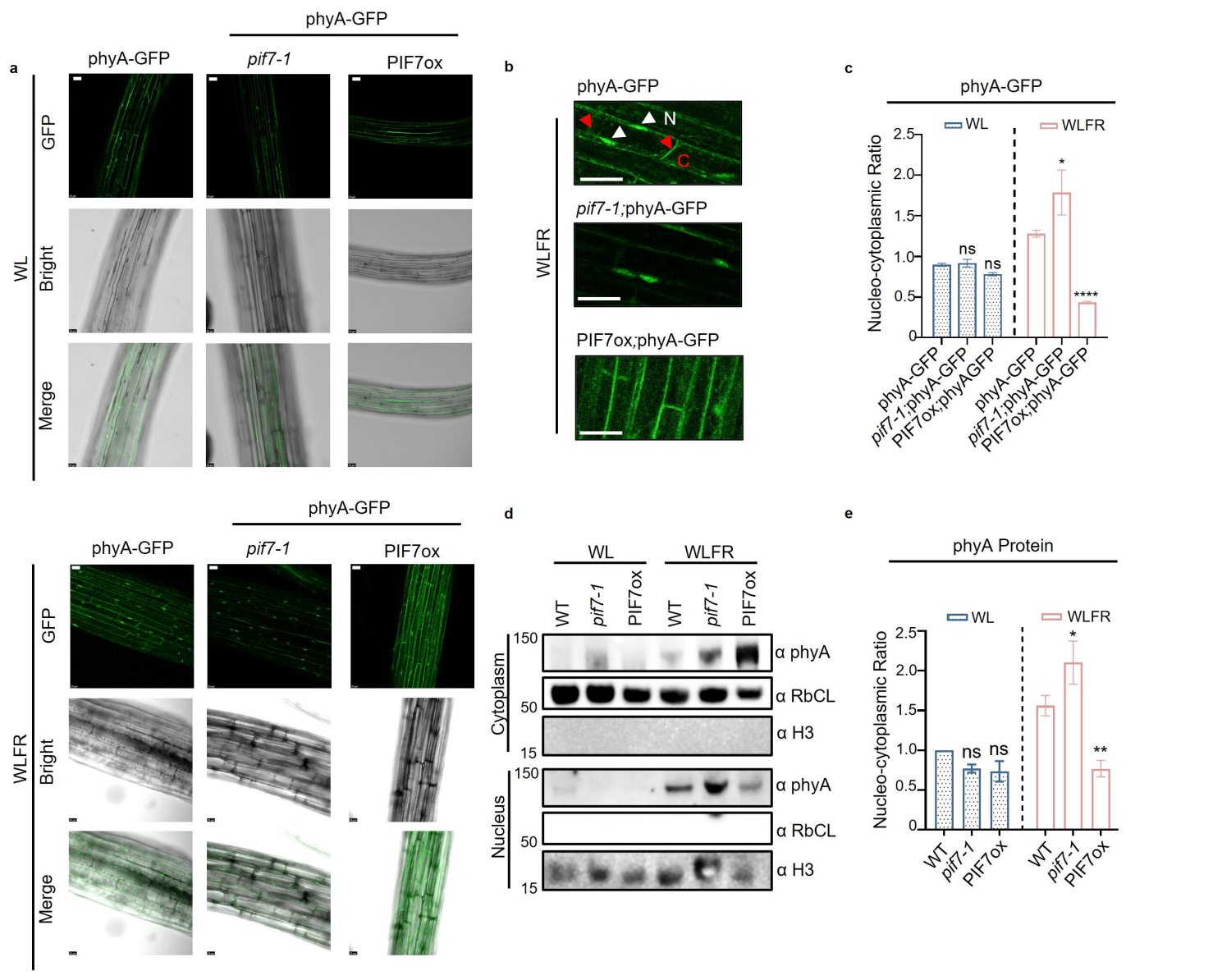

Fig. 4 PIF7 Influences the Sub-cellular Location of phyA

a-c, In WLFR, PIF7ox promotes accumulation of phyA-GFP in the cytosol. Lines of *pif7-1*;phyA-GFP and PIF7ox;phyA-GFP were generated by introgressing *PHYApr*:phyA-sGFP into *pif7-1* and PIF7ox. Close-up images under WLFR are shown in **b**, white arrows and N label indicate nuclear, while red arrows and C label indicate cytosolic signals. In **c**, nuclear/cytosolic (N/C) ratios (relative to WT (*Col-0*), WL control) were calculated following quantification using ImageJ.

d-e, PIF7ox enhances phyA protein accumulation in the cytosol under WLFR conditions. Immunoblot assays were conducted using an anti-phyA antibody, using anti-RbCL as the cytosolic control, and anti-Histone 3 (H3) as the nuclear control. In **e**, cytoplasmic and nuclear phyA was normalised to RbCL and H3, respectively. The N/C ratio for each genotype is shown relative to WT (*Col-0*), WL control. Six-day-old seedlings were sampled as ZT7.

For **a-b** a wavelength of 488nm was used to detect GFP signals. Scale bar=25μm. Representative images from three independent replicates are shown. For **c**,**e**, data are presented as mean values ± s.e.m., n=6 (seedling numbers) in **c**; n=4 (biological repeats) in **e**. A two-way ANOVA test assessed statistical significance between genotypes under WL/WLFR condition (α=0.05); asterisks denote significance compared to the phyA-GFP (phyA N/C) values for WL/WLFR condition(**c**) or phyA protein (phyA N/C) values in WT with WL/WLFR condition(**e**): 0.1234 (ns), 0.0332 (*), 0.0021 (**), 0.0002 (***), $P < 0.0001$ (****).

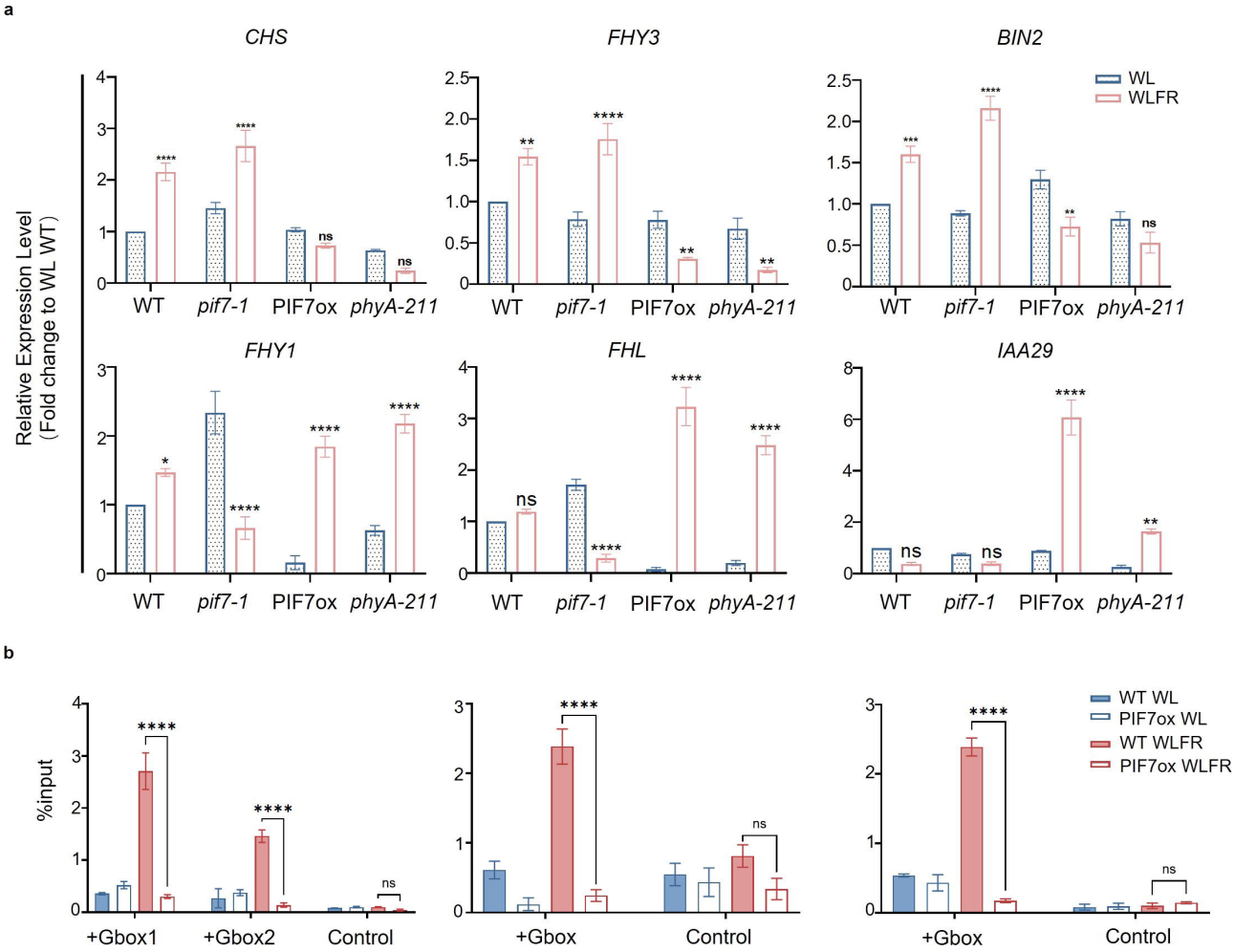

Fig. 5. PIF7 Inhibits phyA-Mediated Regulation of Target Genes

a, qPCR analysis of *CHS, FHY1, FHL, FHY3, BIN2,* and *IAA29* expression in WT (*Col-0*), *pif7-1*, PIF7ox and *phyA-211*. Transcript levels were normalised to the *PP2A* internal control.

b, PIF7ox reduces phyA enrichment at *CHS, FHY1,* and *FHL* promoters under WLFR. Chromatin immunoprecipitation (ChIP)-qPCR was conducted with 6-day-old WT (*Col-0*) or PIF7ox seedlings sampled at ZT7. Native phyA was immobilised on protein A/G beads using an anti-phyA antibody, and promoter enrichment quantified by qPCR at Gbox promoter regions and coding regions, which served as negative controls. Data shown is normalised to input samples.

For **a**-**b**, data are presented as mean values ± s.e.m., n=3 (biological repeats). A two-way ANOVA test was used to assess statistical significance between the WL/WLFR for each genotype (**a**) or different genotypes under the same conditions (**b**) (α=0.05); asterisks indicate statistical significance compared to control: 0.1234 (ns), 0.0332 (*), 0.0021 (**), 0.0002 (***), $P < 0.0001$ (****).

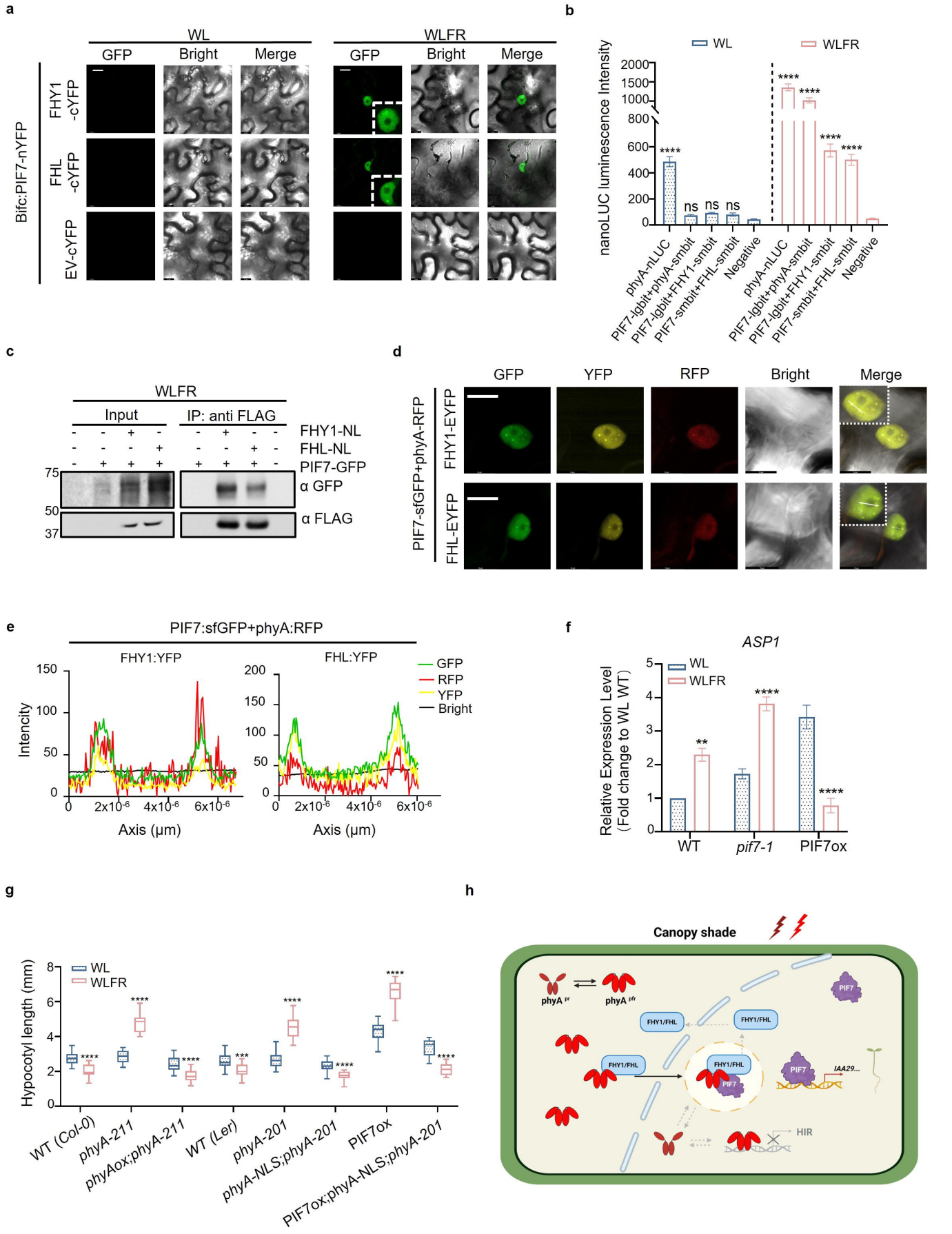

Fig. 6. PIF7 interacts with FHY1/FHL in WLFR

a, The BiFC assay demonstrates PIF7 interaction with FHY1 and FHL. Interaction fluorescence was detected when 35S:FHY1-cYFP (FHY1-cYFP) or 35S:FHL-cYFP (FHL-cYFP) were with expressed 35S:PIF7-nYFP (PIF7-nYFP) in *N. benthamiana* under WLFR.

b, Interactions between PIF7 and FHY1/FHL are detected using a split NanoLUC assay. Strong fluorescence signals were detected between 35S:FHY1-smbitnLUC (FHY1-smbit), 35S:FHL-lgbitnLUC (FHL-lgbit) and 35S:PIF7-lgbit(smbit)nLUC (PIF7-lgbit/smbit) in the transient *N. benthamiana* expression system. The positive controls were phyA-nLUC and PIF7-lgbit+phyA-smbit, while PIF7-smbit+phy-Asmbit was used as a negative control.

c, An immunoprecipitation assay demonstrates PIF7 interacts with FHY1/FHL *in vivo*. 35S:FHY1/FHL-nLUC:3xFLAG-10xHis and 35S:PIF7-sfGFP constructs were transiently expressed in *N. benthamiana* leaves. Anti FLAG beads were used to pull down FHY1/FHL and its target proteins by Co-IP. Anti GFP antibodies revealed GFP-tagged PIF7 co-IP with FHY1/FHL in WLFR.

d-e, Fluorescence assays illustrate that PIF7, phyA and FHY1/FHL co-localise in nuclei and photobodies. 35S driven PIF7-sfGFP, FHY1/FHL-EYFP, and phyA-RFP constructs were transiently expressed in *N. benthamiana* leaves. The merged image (**d**) signifies co-localisation, and **e**, displays GFP, YFP and RFP channel signals relative to white bar shown in the merged nuclear image.

f, PIF7 reduces *ASP1* mRNA levels under WLFR. qPCR analysis of *ASP1* expression in WT, *pif7-1*, PIF7ox, *PP2A* was used as internal control.

g, phyA-NLS is epistatic to PIF7ox. Hypocotyl length (mm) is shown for WT (Col-0), *phyA-211, phyAox;phyA-211,* WT (Ler), *phyA-201, phyA-NLS;phyA-201*, *PIF7ox;phyA-NLS;phyA-201.* Double and triple mutant lines were generated through genetic.

h, Schematic depicting the cellular model for PIF7 control of phyA action in canopy shade. In WLFR PIF7 accumulates in the nucleus, where it interacts with phyA and FHL/FHY1 in photobodies. This sequestration not only blocks phyA from regulating downstream genes but also inhibits its transport into the nucleus. Consequently, PIF7 is able to amplify SAS-mediated hypocotyl elongation by blocking the antagonistic action of phyA. The image created in BioRender (https://BioRender.com).

For **a**,**d**, 488nm and 552nm lasers were used for detecting GFP/YFP and RFP signals. Scale bar=15μm. For **b**,**f**,**g**, data are presented as mean values ± s.e.m., *n*=12 (leaf numbers) in **b**; *n*=3 (biological repeats) in **f**; *n*=24 (seedling numbers) in **g**. A two-way ANOVA test was conducted to determine statistical significance (α=0.05), asterisks denote significance when comparing negative to positive controls and tested interactions (**b**) or compared to WL treatments in each genotype (**f-g**): 0.1234 (ns), 0.0332 (*), 0.0021 (**), 0.0002 (***), $P < 0.0001$ (****).